analytical chemistry

pubs.acs.org/ac Article

High-Throughput μPAD with Cascade Signal Amplification through Dual Enzymes for *arsM* in Paddy Soil

Haorui Cao, Kang Mao,* Jiajia Yang, Qingqing Wu, Jiming Hu, and Hua Zhang*

Cite This: *Anal. Chem.* 2024, 96, 6337−6346 Read Online

ACCESS | Metrics & More | Article Recommendations | Supporting Information

ABSTRACT: The *arsM* gene is a critical biomarker for the potential risk of arsenic exposure in paddy soil. However, on-site screening of *arsM* is limited by the lack of high-throughput point-of-use (POU) methods. Here, a multiplex CRISPR/Cas12a microfluidic paper-based analytical device (μPAD) was constructed for the high-throughput POU analysis of *arsM*, with cascade amplification driven by coupling crRNA-enhanced Cas12a and horseradish peroxidase (HRP)-modified probes. First, seven crRNAs were designed to recognize *arsM*, and their LODs and background signal intensities were evaluated. Next, a step-by-step iterative approach was utilized to develop and optimize coupling systems, which improved the sensitivity 32 times and eliminated background signal interference. Then, ssDNA reporters modified with HRP were introduced to further lower the LOD to 16 fM, and the assay results were visible to the naked eye. A multiplex channel microfluidic paper-based chip was developed for the reaction integration and simultaneous detection of 32 samples and generated a recovery rate between 87.70 and 114.05%, simplifying the pretreatment procedures and achieving high-throughput POU analysis. Finally, *arsM* in Wanshan paddy soil was screened on site, and the *arsM* abundance ranged from 1.05×10^6 to 6.49×10^7 copies/g; this result was not affected by the environmental indicators detected in the study. Thus, a coupling crRNA-based cascade amplification method for analyzing *arsM* was constructed, and a microfluidic device was developed that contains many more channels than previous paper chips, greatly improving the analytical performance in paddy soil samples and providing a promising tool for the on-site screening of *arsM* at large scales.

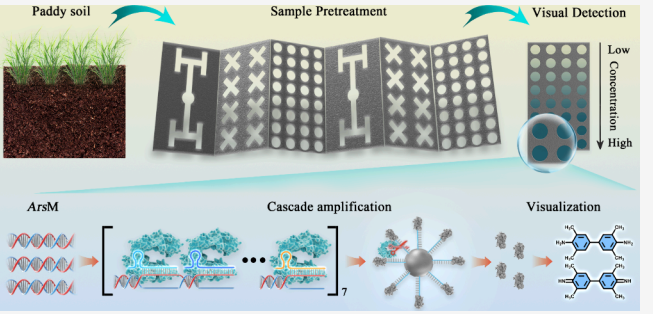

INTRODUCTION

Rice is an important source of arsenic (As) exposure due to its strong ability to adsorb arsenic and important position in the dietary structure. For example, more than 60 million people in Bangladesh are at risk of high arsenic exposure caused by rice consumption.[1−4] Much attention has been focused on the risk of arsenic exposure due to its fatal toxicity, as arsenic has been listed as a class I carcinogen by the World Health Organization and can cause various diseases, such as skin diseases, cardiovascular disorders, and cancer.[5,6]

The risk of As is closely related to its various forms, which usually include inorganic species, such as As(III) and As(V), and organic forms, such as dimethylarsenic (DMA(V)).[7,8] In general, the toxicity of arsenic depends on its chemical form, and the toxicity of the inorganic trivalent form is much greater than that of the organic pentavalent form; for instance, the toxicity of As(III) is 100 times greater than that of DMA(V), and As(III) is among the main sources of arsenic risk in paddy soil.[9−11] Microbial-mediated arsenic methylation is a critical process for the conversion of inorganic arsenic to organic arsenic in paddy soil systems.[6,12] The percentage of methylated arsenics can reach more than 50% in rice.[12,13] Considering that arsenic methylation does not occur in rice plants, microbial methylation is the main source of rice methylated arsenic, and this process is mediated by the arsenite methyltransferase gene (*arsM*).[10,14] The protein expressed by *arsM* can catalyze the methyl transfer from *S*-adenosyl-L-methionine to As(III), forming the intermediate MMA(III), and introduce the next methyl group to form DMA(III), and then conversion to DMA(V) occurs, which could be further methylated to volatile trimethylarsenic for detoxification.[10,15] Moreover, Jia et al. found a significant positive correlation between arsM abundance and methylated arsenic in paddy soil.[7] Therefore, *arsM* is an important biomarker for arsenic methylation in paddy soil systems, and methods to detect *arsM* could provide critical information during investigations on the detoxification of arsenic and help individuals screen for arsenic risks.

Currently, the analysis of *arsM* mainly depends on genome sequencing and real-time fluorescence quantitative PCR (qPCR).[16] The former technique can provide detailed

Received: December 29, 2023
Revised: April 2, 2024
Accepted: April 5, 2024
Published: April 13, 2024

https://doi.org/10.1021/acs.analchem.3c05958
Anal. Chem. 2024, 96, 6337−6346

information on *arsM* sequences, such their classifications, while the latter method can achieve quantitative detection.[7,17,18] However, the wide utilization of these methods for *arsM* screening is limited by several drawbacks, such as their high cost, long testing cycles, high sample requirements, and requirement for ultraclean laboratory conditions; this is especially true for regions and countries with limited resources, such as Bangladesh and Pakistan.[19−21] Moreover, biological samples tend to degrade during transportation and turnover; therefore, developing a user-friendly and economic POU method is critical for *arsM*-based evaluations of potential arsenic risk in paddy soil.

CRISPR is a rising technology that may lead the next generation of nucleic acid POU detection due to its strong specificity, excellent signal transduction ability, and extraordinary reaction compatibility; as a result, CRISPR has received widespread attention.[22] Cas12a is among the most widely used CRISPR toolkits for POU analysis and has demonstrated remarkable performance in the detection of HPV, COVID-19, HIV, *Pseudomonas aeruginosa*, etc.[23−26] For example, Chen et al. constructed the DETECTR method by combining Cas12a with recombinant polymerase amplification and achieved HPV detection at a constant temperature with high sensitivity and specificity.[23] Although Cas12a has already been widely applied in clinical detection, directly applying Cas12a to nucleic acid analysis in environmental samples may be difficult, possibly due to issues with Cas12a, such as insufficient sensitivity.[27] Various studies have attempted to combine Cas12a and preamplification to improve the sensitivity and obtained great achievements; however, due to the saturation reaction in preamplification, quantitative analysis is usually difficult for these methods.[28,29] The qualitative results might be sufficient for the rapid screening of pathogens, but they cannot provide sufficient information for *arsM*-based risk evaluation, which is widely found in paddy soil.

Recently, researchers have also attempted to improve the sensitivity of Cas12a without preamplification, providing hope for the application of this system in the quantitative analysis of targets with low concentrations in environmental samples.[30] These strategies include optimizing the CRISPR/Cas12a system (by introducing coupling crRNA, for example), enhancing the CRISPR/Cas12a system by hydrazone chemistry, and optimizing signal transduction elements, such as decorating ssDNA probes.[31−35] For example, Zeng et al. developed an amplification-free detection platform for ASFV based on a combination of four crRNAs, which improved the sensitivity by 64-fold and could achieve quantitative analysis from 0.0 to 10.0 pM.[31] By first applying hydrazone chemistry to the CRISPR/Cas12a system, Li et al. greatly accelerated the formation of a whole activation strand by exploiting the proximity effect based on base pairing, which activated the CRISPR/Cas12a system quickly and efficiently.[34] The lowest detection limit reached 24 CFU/mL, which was comparable to that of traditional methods.[34] Liu et al. also constructed an electrochemiluminescence biosensor for HPV-16 by anchoring modified probes onto an electrode, which further amplified the detection signal; thus, the LOD decreased to 0.48 pM, and the linear range was 1.0 pM to 10.0 nM.[36] Similarly, Li et al. adopted PbS and CdS quantum dots to construct electrochemical probes and transduce trans-cleavage signals to ratiometric signals, which achieved detection limits of 1.12 and 1.25 cells/mL for Neu5Gc and Neu5Ac, respectively.[37] However, the two strategies are used separately, and it remains unclear whether the methods can be combined to achieve cascade amplification, which may further improve the sensitivity.

In addition to detection methods, the efficiency of pretreatment and determination throughput could limit large-scale, on-site screening of *arsM*. The tedious processes, such as lysis and nucleic acid purification, greatly increase the workload of POU analysis.[38] Recently, paper-based microfluidic chips have been developed that might provide a solution for this issue, for example.[39,40] The device could integrate nucleic acid purification, elution, and distribution of lysate into one paper, which usually consists of capillary forces driving microfluidic channels, which are constructed by wax printing, nucleic acid extraction material, such as glass fiber, and reaction chambers.[20,41] For example, Huang et al. applied μPAD to detect invasive fungi and successfully achieved visible and quantitative POU analysis, greatly improving the portability of the CRISPR system.[42] However, the current paper device only contains a few channels and cannot meet the requirements of large-scale screening due to its enormous spatial heterogeneity in paddy soil.[43,44] Thus, developing a high-throughput paper chip would be beneficial for applying microfluidic paper-based analytical devices (μPADs) in *arsM* POU analysis in paddy soil.

Overall, a coupling crRNA and DNA probe modified by HRP-based cascade amplification was developed and integrated into a high-throughput paper device to achieve large-scale, on-site screening of *arsM*. Different targeted crRNAs were first designed and evaluated for their ability to analyze *arsM*. Then, a coupling system was constructed and optimized by sequentially adding crRNA to lower the background signal and improve the sensitivity. To further improve the sensitivity and visualize the detection results, ssDNA probes modified with HRP and magnetic beads were developed for cascade amplification and signal transduction. Next, a high-throughput paper chip was designed and integrated to simplify the detection process and reduce the workload; this process was based on a channel cascade amplification strategy, after which the reactions were integrated into the device. Finally, this platform was applied in the POU analysis of *arsM* in Tongren City, China, to further verify its reliability. The relationships between *arsM* abundance and environmental factors were also explored based on the results. We aimed to develop a high-throughput detection platform with excellent sensitivity, low background signals, and strong specificity that offers a promising method for *arsM* POU analysis in paddy soil.

EXPERIMENTAL SECTION

Materials. The crRNAs were synthesized by Biolife Sci (China). $MgCl_2$, GuSCN, and BSA were purchased from Sigma (Germany), and $NaHCO_3$ and azido-PEG4-NHS ester were purchased from Aladdin (China). Kanamycin and PBS were purchased from Solebao (China), and magnetic beads (MBs) were purchased from Biotyscience (China). Ultrapure DNase/RNase-free distilled water, horseradish peroxidase (HRP), TMB chromogenic agent, and optical adhesive film were obtained from Thermo Fisher Scientific (USA). Plasmids were synthesized by Genewiz (USA), while ssDNA probes were obtained from Sangon Biotech (China). The plasmid small extraction kit was obtained from Tiangen (China). Filter paper and glass fiber were obtained from Whatman (USA). Wax was purchased from Xerox (USA). The sequences of the nucleic acids are shown in Table S1.

https://doi.org/10.1021/acs.analchem.3c05958
Anal. Chem. 2024, 96, 6337−6346

Preparation of *arsM*. The *arsM* sequences were obtained by performing genome sequencing of paddy soil and NCBI comparisons. Then, the sequence with the highest relative abundance was selected as the target, which belonged to Bacteria, Bacillota, Clostridia, Peptostreptococcales, Peptostreptococcaceae, and Paraclostridium. The plasmid constructed by Genewiz (USA) was first transfected into competent DH5α cells by the heat shock method. Afterward, 50 μL of bacterial solution was inoculated into an LB agar medium supplemented with 50 mg/L kanamycin. Then, an adequate colony was selected after incubation overnight at 37 °C, and 100 mL of liquid LB medium supplemented with 50 mg/L kanamycin was added. Finally, the bacteria were harvested after incubation overnight, and the plasmid was extracted via a plasmid small extraction kit according to the manufacturer's instructions. The plasmid was stored at −80 °C until use, and its concentration was determined with a Qubit 4.0.

Construction of the Cas12a Reaction. Next, 1 μL of the Cas12a-crRNA premix solution containing 1 μM Cas12a and 1.25 μM crRNA in a 1× NEB buffer 2.1 was added to 17 μL of 1× NEB buffer 2.1 containing different concentrations of the *arsM* plasmid. Then, 2 μL of 5 μM ssDNA fluorescent probes was added to the solution to construct a 20 μL reaction system. Afterward, the solutions were placed into a qPCR instrument (ABI7500), and the reaction mixture was incubated at 37 °C for 1 h. The fluorescence signal was recorded every 1 min.

Construction of the Coupling crRNA System. We prepared different Cas12a-crRNA premixes according to Construction of the Cas12a Reaction, followed by mixing of the solutions that were utilized to construct the coupling system in equal proportions. Then, we added 1 μL of mixing solution to 17 μL of 1× NEB buffer 2.1 containing different concentrations of the *arsM* plasmid and added 2 μL of 5 μM ssDNA fluorescent probes. Finally, the reaction was conducted in a PCR instrument at 37 °C for 1 h, and the fluorescence signal was recorded every 1 min.

Preparation of HRP-ssDNA-MB Probes. First, we prepared a 50 μM HRP solution by dissolving 2 mg of HRP in 1000 μL of 0.1 M $NaHCO_3$ solution. Then, 1000 times excess azido-PEG4-NHS ester linkers were added to the HRP solution and incubated at room temperature for 2 h. Then, excess azido-PEG4-NHS ester linkers were removed via a desalting column. The modified HRP was then concentrated by ultrafiltration. Afterward, 200 μL of 10 μM azido-modified HRP was added to 2 equiv of 5′-DBCO TEG-T_{25}-biotin-3′ DNA, followed by incubation for 15 h in PBS. The excess DNA was then removed by ultrafiltration.

Next, 40 μL of streptavidin-modified magnetic beads was added to 600 μL of PBS buffer containing 0.1% Tween 20, followed by the addition of 5 μL of 800 nM HRP-DNA-biotin. The mixture was shaken at 1500 rpm for 5 min, followed by centrifugation at 20,000 rpm for 1 min to remove the supernatant. Finally, the modified MBs were washed at least 10 times to thoroughly remove the residual HRP.

Construction of a Cascade Amplification Platform Based on Coupling crRNA-HRP. A coupling crRNA mix was prepared according to Construction of the Coupling crRNA System, and then 5 μL of the mixture and an adequate volume of 1× NEB buffer 2.1 were added to the modified magnetic beads. The solution was then divided into four tubes after being fully mixed. Next, different concentrations of plasmid in 1× NEB buffer 2.1 were added to the tube, followed by dilution to 60 μL. Then, the reaction was incubated at 37 °C for 40 min, and the supernatant was obtained via centrifugation. Finally, 30 μL of the supernatant was transferred to 30 μL of TMB, and the fluorescence was recorded at an excitation wavelength of 570 nm and an emission wavelength of 575 nm according to Samanta et al.'s research.[45] For the colorimetric method, the color was recorded by a mobile phone and extracted via ImageJ.

Fabrication of the μPAD Device. The paper chip of the μPAD device was designed by CorelDRAW 2022, and a detailed illustration is shown in Figure S5. After designation, the image was converted into a PDF file, followed by single-page printing via a wax printer (Xerox Colorqube 8570) with filter paper (A4 size). The printed paper was then heated by a hot plate at 120 °C for 2 min while the paper was shaken slowly to fully infuse the wax into the paper. Then, we prepared glass fiber circles by creating holes with a 5 mm punch. Finally, the glass fiber circles were placed on the paper chip in Part 4 in Figure 3 for use.

The PMMA plate of the μPAD device was designed via RDworks with a length of 80 mm and a width of 44 mm. The thickness of the plate was 5 mm. The diameter of the reaction chamber was 5 mm, and its distribution was the same as that of Part 1 in Figure 3. After designation, the plate was fabricated by a laser cutting machine with a cutting speed of 0.48 mm/s and a 94% maximum power. Finally, one side of the plate as the bottom was sealed for utilization.

Sample Collection and Analysis. Soil samples were collected from Wanshan, Tongren, China, and were stored according to the testing indicators. The samples used to determine biological indicators were stored in liquid nitrogen and transferred to −80 °C after being transported to the laboratory until use. For environmental indicators, the samples were stored at 4 °C and ground via an agate mortar after freeze-drying. For the analysis of trace elements, total organic carbon (TOC), and total nitrogen (TN), samples were sieved through 200 mesh, while they were sieved through 10 mesh for pH detection.

For the on-site screening of *arsM*, soil samples were first collected via a five-point sampling method to avoid errors caused by soil heterogeneity. After collection, impurities such as rice roots and stones were removed carefully. Then, approximately 1 g of soil was ground with the help of a magnetic oscillator and quartz sand, followed by lysis according to a commercial kit (Qiagen Powersoil Kit). Then, the lysates were added to glass fiber circles one by one. Afterward, the paper was folded according to step 3 in Figure 3, and 80% ethanol was added at least twice to remove the impurities. After washing was performed, the paper was moved to the upper part of the PMMA plate and the folding method was conducted as described in step 4 in Figure 3. Then, TE buffer was added to elute the DNA from the glass fiber circles to the reaction chambers. Next, the reaction reagents were added to the chambers, and the plate was sealed for Cas12a recognition and cleavage. After incubation at 37 °C for 40 min, the supernatant was transferred to another PMMA plate for color reaction. A colorimetric method was used to read the results via ImageJ. Four parallel reactions were performed for each sample, which were distributed in one column.

Trace elements were analyzed by ICP−MS. First, 50 mg of sieved soil was transferred to Teflon tubes, followed by the addition of 3 mL of HNO_3 and 0.5 mL of HF. The tubes were then put into a baking oven and incubated at 150 °C for 48 h.

https://doi.org/10.1021/acs.analchem.3c05958
Anal. Chem. 2024, 96, 6337−6346

Scheme 1. Principle of the Coupling crRNA-HRP-Based Analysis Platform[a]

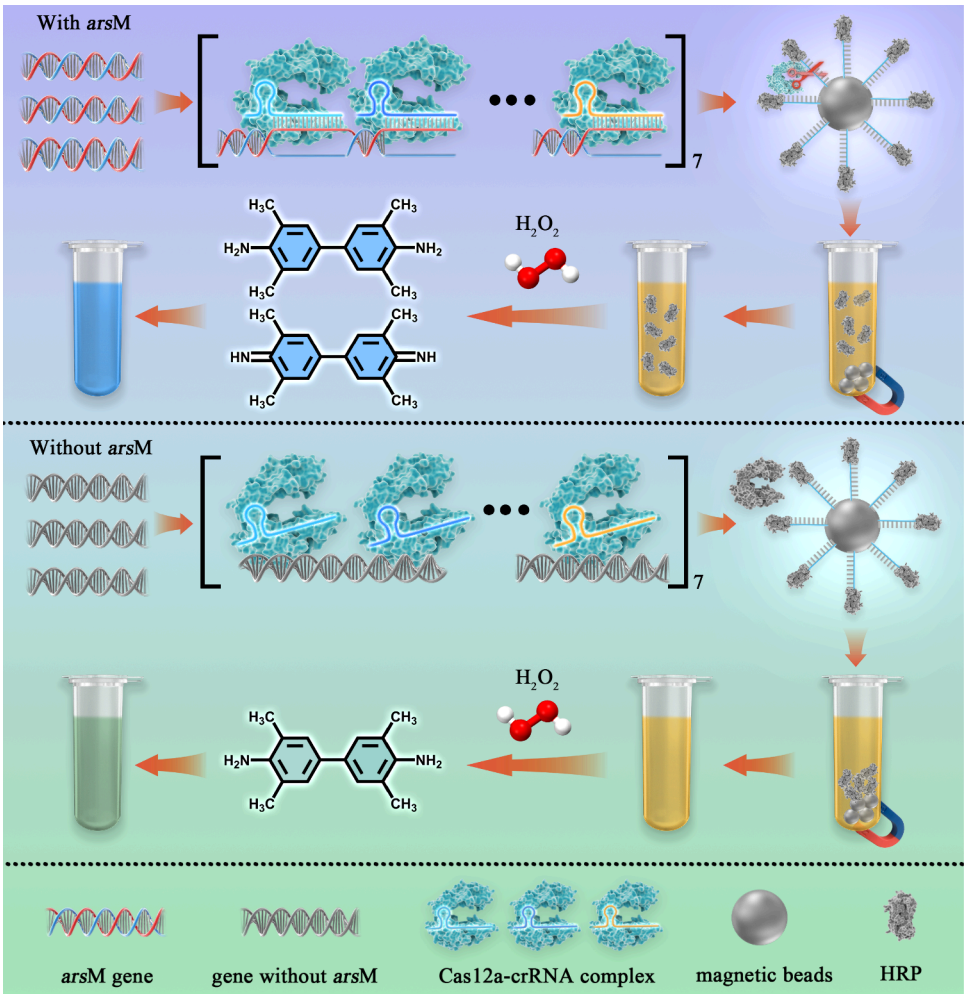

[a]In the presence of *arsM*, Cas12a-crRNAs recognize the target sequences, and their trans-cleavage activities are activated. The ssDNA-linked magnetic beads and HRP were then cleaved, followed by separation. Next, under magnetic force, the beads remained at the bottom, while HRP remained in the supernatant. Finally, the supernatant was transferred to the TMB solution, and the color changed to blue rapidly. However, in the absence of *arsM*, the complex could not be activated, and HRP was still linked to the beads. Therefore, HRP could not enter the supernatant under magnetic force. The color of TMB did not change because there was no HRP.

Next, 1 mL of H_2O_2 was added to the tube and left to react at 90 °C for 1 h, after which the acid was left to dry until HF was removed. Afterward, 0.2 mL of HNO_3 and 1.8 mL of DDW were added to the tube and incubated at 150 °C for 6 h. Finally, the solution was transferred to a centrifuge tube and diluted to 10 mL. The solution was stored at 4 °C until further tests were performed.

The pH was determined with a portable pH meter (INESA Scientific Instrument Co., Ltd., Shanghai). Approximately 10 g of soil samples sieved through 10 mesh was first transferred to 50 mL centrifuge tubes, followed by the addition of 25 mL of DDW. Then, the samples were vibrated for 10 min. The samples were then left to stand until they cleared, after which the electrode was inserted into the supernatant and the values were recorded. TOC and TN were determined by an elemental analyzer (Germany). Two grams of soil was first added to 15 mL centrifuge tubes, followed by the addition of 2 M HCl. After reaction for 7 h, the excess acid was removed by washing with DDW. Then, the samples were freeze-dried and ground. Finally, the ground samples were wrapped in aluminum foil for testing.

RESULTS AND DISCUSSION

Sensing Principle. The sensing principle of the platform is shown in Scheme 1. In the presence of *arsM*, the crRNA guided Cas12a to recognize the target fragment and perform cis-cleavage. Then, the trans-cleavage activity of the complex was activated, and ssDNA probes were cleaved with a much higher efficiency, which can transduce and amplify the signal simultaneously. Then, different crRNAs were introduced into the system to construct a coupling system and improve the sensitivity. Next, the enzyme-modified probes were applied to the reaction mixture to achieve cascade amplification and visualization detection. HRP was selected as a reporter due to its great stability and excellent signal amplification capability, and HRP was connected to MBs via ssDNA. Therefore, different activated Cas12a-crRNA complexes cleaved the ssDNA-connected HRP and MBs efficiently. Under magnetic force, the MBs were absorbed to the bottom, while the separated HRP remained in the supernatant. The supernatant was then transferred to the TMB solution, and the mixture was catalyzed to blue, which could be observed directly via the naked eye.[34,46] Conversely, Cas12a-crRNA complexes were

https://doi.org/10.1021/acs.analchem.3c05958
Anal. Chem. 2024, 96, 6337−6346

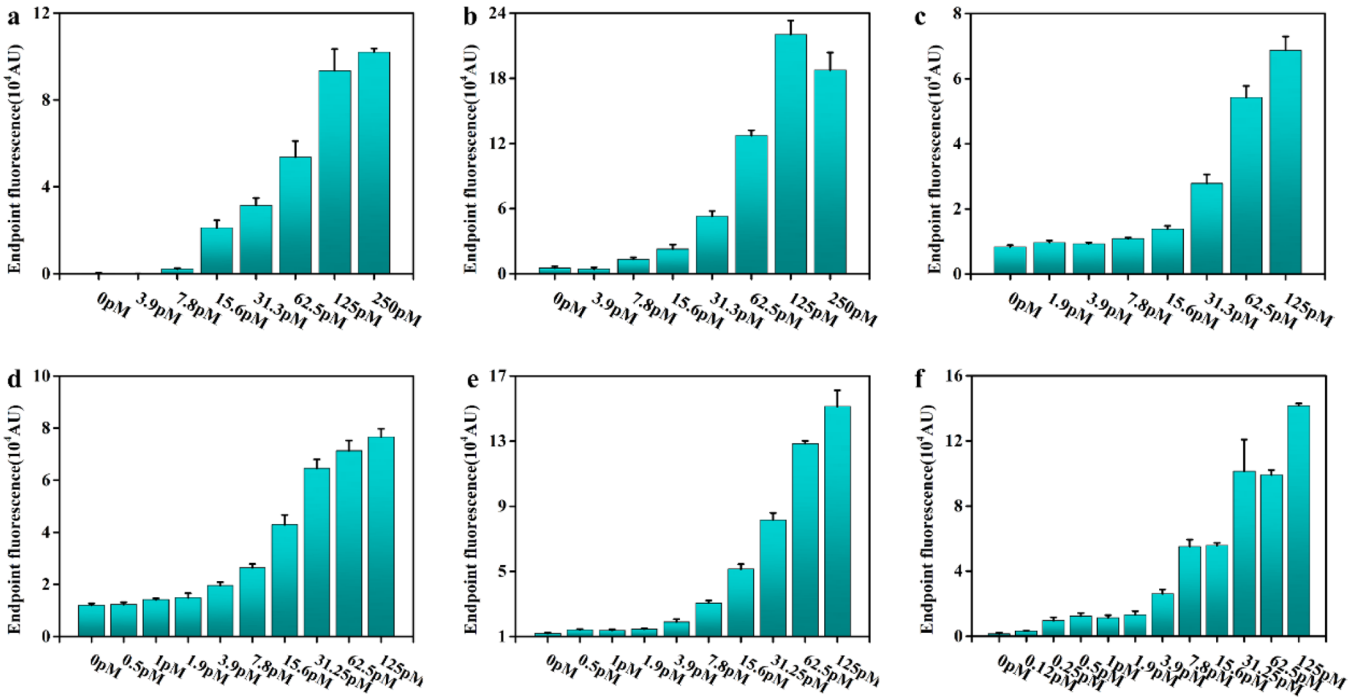

Figure 1. End point fluorescence for *arsM* detection based on the coupling crRNA system. (a−f) End point fluorescence curve for *arsM* detection based on the crRNA 1−2, crRNA 1−3, ..., and crRNA 1−7 coupling systems.

silenced when no *arsM* was present, while HRP and MBs could not be separated. Thus, HRP was also present at the bottom of the tube under the external magnets, and TMB could not be catalyzed to blue because there was no HRP in the supernatant.

Construction and Optimization of the Coupling crRNA System. Seven crRNAs that target different regions of *arsM* were first designed according to *arsM* sequences and the recognition principle of Cas12a. Gradient concentration plasmids with 2-fold serial dilutions were adopted to evaluate their sensitivities and background signals. As shown in Figures S1 and S2, the background signals were low except for crRNA6. The sensitivities of the complexes were similar and between 3.9 and 7.8 pM, which were lower than those in previous studies.[31,47] Therefore, the crRNAs designed in this study were sensitive and had a low background signal, which provided a great basis for the construction of a coupling system.

Then, six coupling methods with different amounts of crRNAs were constructed via a step-by-step iterative approach to explore whether increasing the number of crRNAs can continuously improve the sensitivity of the CRISPR/Cas12a detection system. As shown in Figure 1a,b, coupling of crRNAs 1 and 2 or 1, 2, and 3 did not improve the sensitivity or decrease the background signal. When crRNA 4 was further introduced, the LOD decreased from 7.8 to 1.9 pM. Interestingly, the further introduction of crRNAs 5, 6, and 7 also improved the sensitivity and achieved the greatest sensitivity when coupling all crRNAs, which had a detection limit of 0.12 pM. Notably, the detection limit of this coupling method was 32 times lower than that of the most sensitive complex, Cas12a-crRNA7. Apart from sensitivity, as shown in Figures S1 and S3, the coupling method could also improve the reaction speed, which could reach saturation in a shorter time (at least 10 min earlier than the noncoupling system). For the detection of samples with low contents of *arsM*, the slopes of the fluorescence curves were also greater. Moreover, introducing crRNA 7 to the coupling method decreased the background signal significantly (from 1.2×10^4 to 1.4×10^3), which might greatly improve the cascade amplification performance because the background signal might be amplified in follow-up reactions.

The reasons for the phenomenon are then discussed. Introducing crRNAs 2 and 3 did not always improve the sensitivity of the coupling system, indicating that the crRNAs involved in the combination may need to meet certain conditions (Figure 1a,b). The addition of crRNAs 4−7 decreased the detection limit, while their sensitivities were similar to, lower than, or higher than those of previous crRNAs, suggesting that the sensitivity of crRNA is not the key factor. Moreover, as shown in Figure S1, the trans-cleavage efficiency was not the critical influence for improving the sensitivity. For example, crRNAs 1 and 2 possessed a high trans-cleavage efficiency, while their combination had little influence on the detection limit. In contrast, crRNAs 3 and 5 had a low trans-cleavage ability, and the former could not influence the detection limit; however, the latter could improve the sensitivity significantly. As the two important features of the complex were not critical factors that could influence the sensitivity of the coupling system, the synergistic effect between different complexes might cause an improvement in sensitivity. However, further research is needed to clarify the conditions that trigger this synergistic effect. The background signal of the coupling system was also unrelated to those of the involved complexes. For example, no background signal was observed for crRNAs 4 and 5, but the background signal was increased when these components were introduced into the coupling method. Conversely, crRNA 6 exhibited high fluorescence without a target, but its addition to the coupling system significantly decreased the background signal significantly. Above all, the detection performance of the coupling system mainly depends on interactions between complexes

https://doi.org/10.1021/acs.analchem.3c05958
Anal. Chem. 2024, 96, 6337−6346

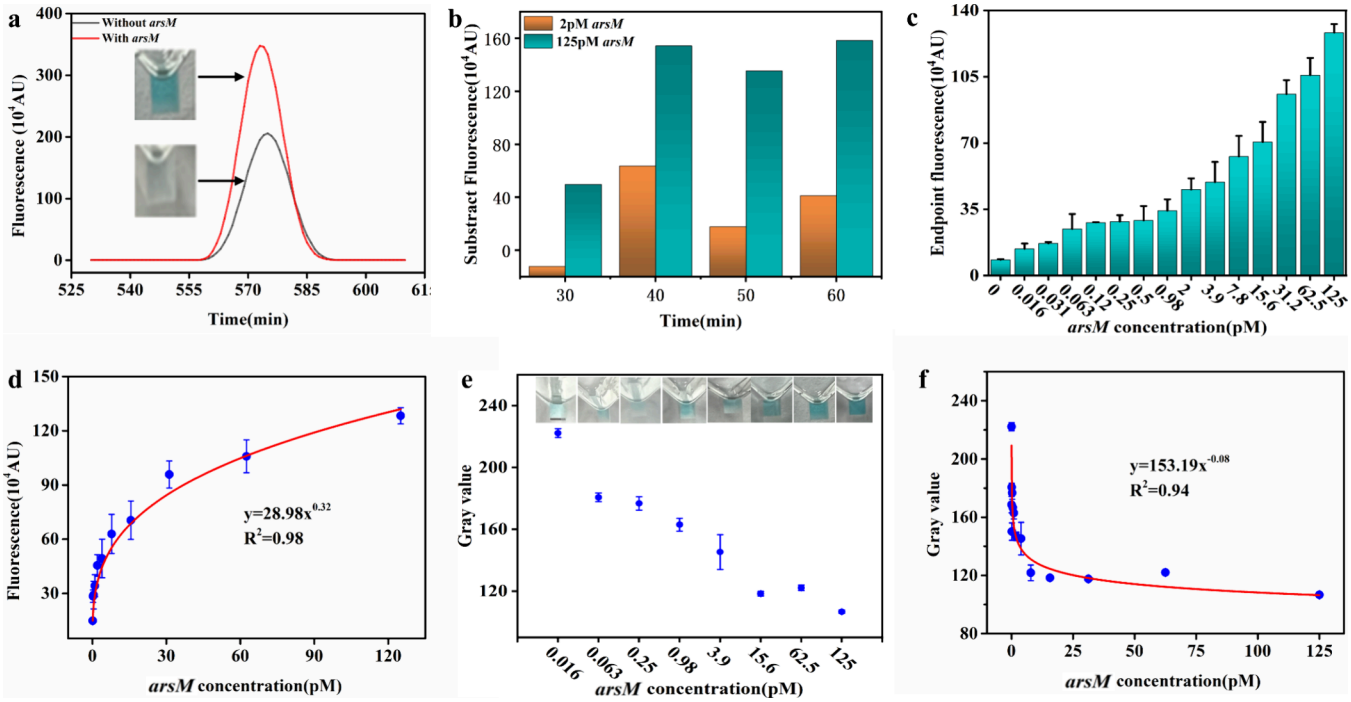

Figure 2. Feasibility analysis, time optimization, and detection performance of the coupled crRNA system-HRP-based platform. (a) Fluorescence and color detection with or without *arsM*; (b) end point fluorescence of samples with low or high concentrations of *arsM* under different reaction times; (c) end point fluorescence of detection results for *arsM* between 125 pM and 16 fM with 2-fold serial dilution; (d) nonlinear fitting curve between the *arsM* concentration and fluorescence; (e) colors and extracted gray data of the *arsM* detection results; (f) nonlinear fitting curves between the *arsM* concentration and gray data.

rather than their properties, such as sensitivities and trans-cleavage activities. The factors that influence this interaction effect may require further research.

Construction and Optimization of HRP-Based Cascade Amplification. Considering the low abundance of *arsM* in paddy rice and limited on-site detection abilities, we developed HRP-ssDNA-magnetic bead probes to further amplify the *arsM* signals and achieve a visualized detection. The reaction was first constructed according to the coupling system, while the probes were changed to HRP probes. Samples without *arsM* and with 125 pM *arsM* were utilized to assess the reaction, and the results were observed via fluorescence and colorimetric methods. As shown in Figure 2a, the experimental group demonstrated a significantly darker color and a much higher fluorescence value at 575 nm than that of the control group, verifying the feasibility of the current method for detecting *arsM*.

As real-time monitoring is difficult to achieve during on-site analysis, end point detection might be more adequate. The reaction time is critical for the detection performance of end point analysis. The sensitivity was too low when the reaction time was short, while the reaction reached saturation, and the quantitative ability decreased when the time was too long. Therefore, time optimization was conducted. As shown in Figure 2b, there was no fluorescence in samples with 2 pM *arsM* after the background was deducted when the reaction time was 30 min, and the fluorescence values remained low even in samples with high contents of *arsM*. The signal in samples with low and high concentrations of *arsM* increased greatly when the reaction time was extended to 40 min. The signal strength of the former could even exceed that of samples with high concentrations of *arsM* over 30 min. For the latter, the fluorescence signal increased more than 300% compared with that at 30 min. However, further increasing the reaction time did not improve the signal intensity in samples with both high and low concentrations of *arsM*, indicating that the reactions reached saturation. Thus, 40 min was selected as the optimal time.

Then, the quantitative range and detection limit of the method were assessed. As shown in Figure 4c, the platform exhibited a great quantitative capability between 16 fM and 125 pM (r^2 = 0.98) with a LOD as low as 16 fM, which was 8 times lower than that of the coupling method. Interestingly, the concentration-signal effect was not great before the HRP probes were introduced. This phenomenon might be caused by two factors. First, the platform possessed a shorter reaction time, avoiding reaction saturation. Second, the cascade amplification strategy further expanded the variations in the ssDNA cleavage rate caused by concentration differences and better reflected the concentration variations. Then, the colorimetric detection performance was explored due to its convenience in POU analysis. As shown in Figure 2e,f, the sensitivity of the colorimetric method reached 16 fM. The color of the TMB solution became darker with increasing amounts of *arsM*, indicating a great concentration-color effect. Then, the colorimetric signal was extracted via ImageJ, and r^2 reached 0.94, demonstrating an excellent quantitative ability. Notably, the fitting curves between the fluorescence or gray data and the *arsM* concentration were exponential functions, which indicated that the cascade amplification effect was generated by the combination of the coupling system and HRP probes. The exponents of the exponential function are less than 1, which may result from the gradual saturation of the HRP color as the *arsM* concentration increases.

Overall, the introduction of HRP into the platform improved the sensitivity and response to variations in the sample

https://doi.org/10.1021/acs.analchem.3c05958
Anal. Chem. 2024, 96, 6337−6346

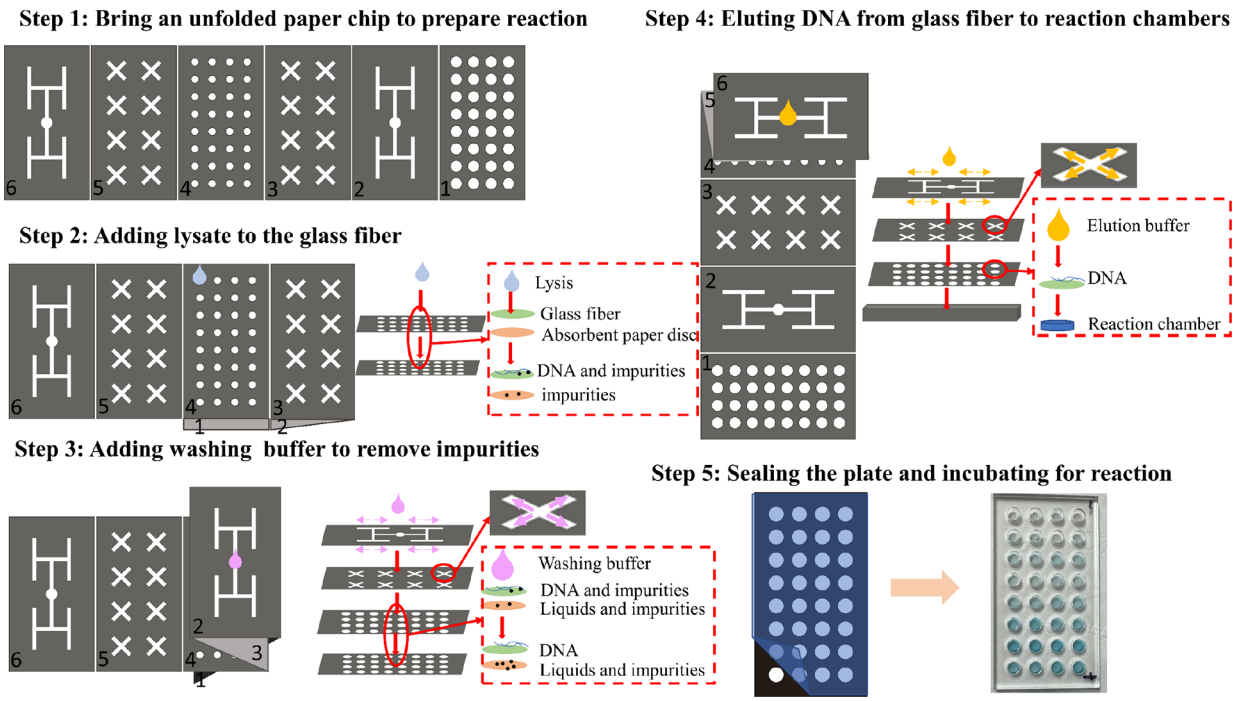

Figure 3. Principle and folding procedures for μPAD as well as colorimetric readouts generated by TMB oxidation. A paper device was fabricated via wax printing. The black region was a hydrophobic area immersed in wax and was utilized to constrain the fluid. The white region represents the filter paper without wax, and it was utilized as the migration channel of the fluid. For utilization, first, an unfolded paper chip is brought and folded according to step 2. Next, the lysate was added to the glass fiber in region 4, followed by folding of the paper as described in step 3. Then, impurities were removed by the addition of washing buffer at least twice. After completely drying the glass fiber, the paper was folded as described in step 4, followed by the addition of elution buffer to transfer the DNA into the microfluidic plate. Finally, the plate was sealed for reaction.

concentration, and the platform exhibited a quantitative ability as a result. Compared with that of previous studies, our developed method possessed excellent quantitative performance with great sensitivity (Table S2). Moreover, the results could be read with fluorescence or colorimetric methods, providing diversification signal readout routines for POU analysis.

Fabrication of a High-Throughput μPAD Device. Although the reactions constructed above overcame the requirements for thermal cycles and precise signal readout equipment, tedious pretreatment processes and limited analysis throughput restrain their utilization in POU analysis. Therefore, μPAD was introduced to the platform to address these drawbacks.

A representation of the paper device is shown in 3 and Figure S5, which consisted of a paper chip and PMMA plate, while the actual device is shown in Figure S4. The paper chip was formed by the hydrophilic white region and the hydrophobic black region, which were immersed in wax. The liquid is driven along the white channel due to capillary force, and its detailed routine is marked in Figure 3. The latter was fabricated via a laser cutting machine and utilized to incubate the reactions. The throughputs of previous paper chips were usually three to five and could test only a few samples simultaneously, which could not satisfy the requirements for large-scale screening in previous publications.[39,48] In this study, the cascade amplification approach was introduced into the design of μPADs, and the throughput was increased to 32, which greatly improved existing devices and successfully overcame throughput issues. As shown in Figure 3, the reagent is uniformly dispersed to eight end points, and this process is driven by capillary action after the reagent is added from 2 or 6 circular pores. As the eight end points corresponded to the center of the X-shaped channel of layer 1 or layer 5, the solution was further divided into four parts and formed 32 channels.

Then, samples spiked with different concentrations of plasmids were utilized to verify the feasibility of the device and determine its sensitivity, background signal, and recovery rate, and the visual readout is shown in Figure S4. The sample with 16 fM *arsM* could trigger a colorimetric signal that was observable via the naked eye, and there was no signal in the control group (Figure S4). Then, spiked experiments were conducted to explore the performance of the device with real soil samples. As shown in Table S3, the recovery rate ranged from 87.70 to 114.05%, demonstrating great quantitative accuracy in POU analysis, which could fully meet the requirements of on-site screening. Then, we compared the detection performances of μPAD and those without the use of μPAD (traditional PCR tubes). According to the above results, μPAD could detect samples with *arsM* concentrations as low as 16 fM, which is similar to the sensitivity of PCR tubes. The quantitative results obtained for μPAD were close to the spiked concentration, indicating the great accuracy of μPAD; this result was similar to that in PCR tubes, which could be demonstrated by the high r^2 value obtained in the linear fitting curve without μPAD. The stability of μPAD was also comparable to that of traditional devices, as demonstrated by the small RSD (Table S3) with μPAD and the error bar without μPAD (Figure 2). Above all, the comparable detection performance between utilizing μPAD and utilizing traditional devices demonstrates the great compatibility between the reaction and μPAD.

https://doi.org/10.1021/acs.analchem.3c05958
Anal. Chem. 2024, 96, 6337−6346

Table 1. *arsM* Abundance and Environmental Factors in the Paddy Soil of the Wanshan District of Tongren City in China

Log_{10} (*arsM* (copies/g))	Cr (mg/kg)	As (mg/kg)	Se (mg/kg)	Cd (mg/kg)	Sb (mg/kg)	Pb (mg/kg)	pH	TN (%)	TC (%)	TOC (%)
7.41	103.08	30.73	2.96	0.65	4.24	76.00	8.03	0.27	3.87	2.00
6.68	78.67	23.69	2.41	0.56	3.70	63.39	8.01	0.26	3.90	1.95
7.40	88.57	25.92	3.71	0.54	3.38	68.74	7.76	0.27	4.02	2.00
7.81	92.02	28.86	2.90	0.66	5.26	76.14	7.82	0.28	4.00	2.04
7.24	73.02	42.32	5.41	0.38	6.63	102.81	5.53	0.18	1.57	1.52
6.95	74.93	46.50	5.98	0.44	7.51	103.23	5.48	0.26	2.33	1.75
7.25	78.60	19.35	2.56	1.62	4.63	55.45	7.73	0.26	3.50	1.80
7.39	92.46	23.91	3.75	1.90	5.49	65.78	7.65	0.27	3.52	1.81
6.02	67.25	30.33	2.56	1.43	3.73	54.90	7.86	0.23	3.86	1.57
7.57	69.30	30.15	3.20	1.37	3.84	54.83	7.95	0.23	3.87	1.61
7.45	80.22	25.85	3.24	1.16	13.04	54.76	6.10	0.26	2.34	1.92
7.27	91.31	28.68	4.25	1.28	14.27	61.15	6.12	0.25	2.33	1.96
6.03	72.33	25.89	3.64	0.89	12.82	55.10	7.45	0.27	2.85	2.01
6.93	85.50	30.37	3.15	1.01	15.98	62.82	7.36	0.26	2.87	1.87
7.14	49.35	19.79	12.72	1.39	20.37	45.46	7.49	0.18	4.90	1.68
7.25	63.04	25.17	11.14	1.93	29.02	55.35	7.43	0.18	4.89	1.67

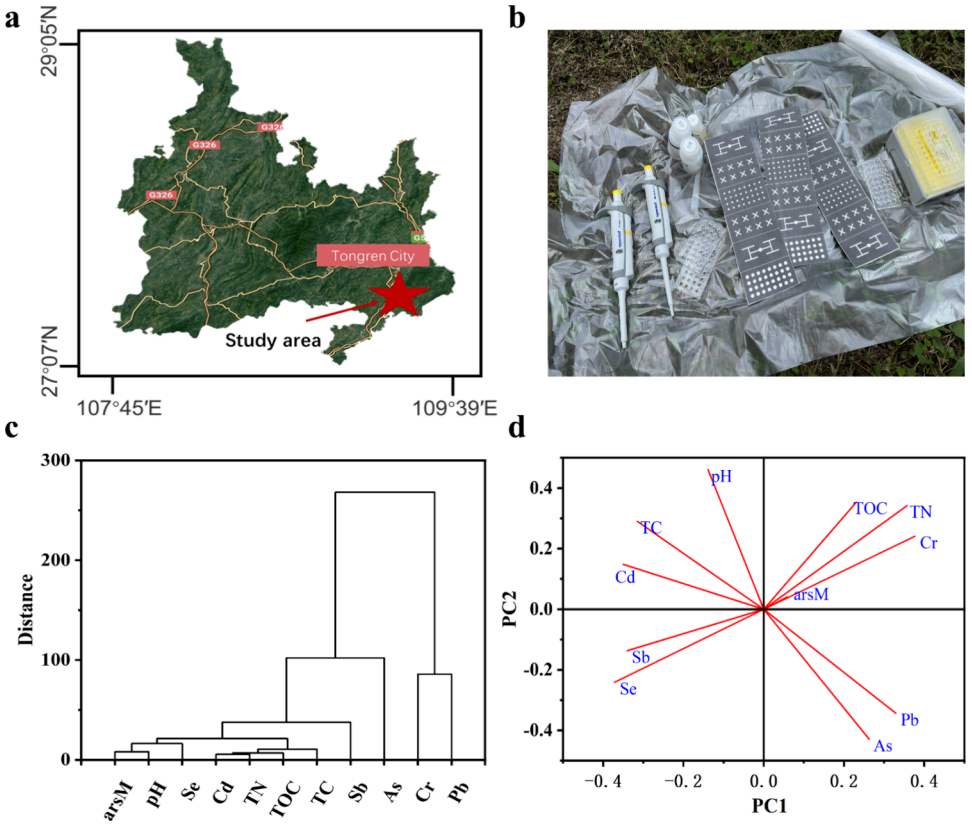

Figure 4. POU analysis of *arsM* and its relationship to environmental indicators. (a) Position of the study area, (b) preparation for on-site detection, (c) systematic clustering analysis for *arsM* and environmental indicators, and (d) principal component analysis that was carried out for *arsM* and environmental indicators.

Then, we evaluated the cost of the detection platform, which is critical for on-site large-scale screening. As shown in Table S4, the cost for each reaction based on the cascade amplification μPAD device was 2.12 dollars, which was inexpensive for large-scale *arsM*. Therefore, the device developed here is inexpensive and exhibits high compatibility, great efficiency, and excellent operability, making it a promising technique for high-throughput POU analysis.

Evaluation of *arsM* in Paddy Soil. Finally, the platform was used to perform the on-site screening of *arsM* in paddy soil. We selected 16 sites in Wanshan, Tongren City, which are marked in 4a. Four parallel samples were utilized for quality control, and a colorimetric method was utilized to analyze the abundance. As shown in Table 1, *arsM* was detected successfully, and its abundance was between 1.05×10^6 and 6.49×10^7 copies/g; an average of 1.97×10^7 copies/g was attained. The application further verified the feasibility of the method in the on-site analysis of real samples.

Then, environmental factors were further detected in the paddy soil samples, as shown in Table 1. First, systematic clustering and principal component analysis (PCA) were used to explore the environmental factors that could influence the

https://doi.org/10.1021/acs.analchem.3c05958
Anal. Chem. 2024, 96, 6337−6346

abundance of *arsM*. As shown in Figure 4c, no significant relationship was observed between most indicators and *arsM*. The relationship between *arsM* and As also appeared to be insignificant, possibly because the variation in As content was small, which could not influence the abundance of *arsM*. Similarly, the PCA results also demonstrated that these indicators could not greatly influence the abundance of *arsM*. We selected pH and Se, which are similar to those of *arsM* according to the systematic clustering results. Linear and nonlinear correlation analyses also demonstrated that these parameters weakly influenced the abundance of *arsM* (Figure S6). Therefore, these environmental indicators had little influence on the abundance of *arsM* in the study area.

Above all, *arsM* was successfully detected via a multiplex μPAD device based on cascade amplification, which was driven by a coupling crRNA system and HRP-modified MBs; thus, this device provided abundant information in the study area, demonstrating its enormous potential for POU analysis and screening of potential risks of arsenic.

CONCLUSIONS

This study first developed a coupling crRNA-HRP-based cascade amplification μPAD for *arsM* detection with a detection limit of 16 fM, a dynamic range of up to 5 orders of magnitude (16 fM to 125 pM), a low background signal, high throughput (up to 32 detection channels), and quick testing time (1 h). Moreover, the reaction was conducted at a constant temperature, and the results could be observed via the naked eye. In addition, μPAD was very inexpensive, significantly decreasing the detection cost. The screening of *arsM* in paddy soil demonstrated that μPAD was very reliable in real sample analysis. Due to its modular assembly strategy, the platform could also be applied for other nucleic acid biomarkers by replacing crRNAs in the environment, which further demonstrated its great potential for high-throughput POU analysis.

ASSOCIATED CONTENT

Supporting Information

The Supporting Information is available free of charge at https://pubs.acs.org/doi/10.1021/acs.analchem.3c05958.

Sequences of *arsM*, gRNA, and ssDNA linking HRP and MBs, comparison of detection performance between this method and other assays, recovery rate of spiking experiments, real-time fluorescence curves and end point fluorescence for *arsM* detection based on Cas12a-crRNA1−7, real-time fluorescence curves for *arsM* detection based on coupling systems, detection results of *arsM* based on the colorimetric method via the μPAD device, designation of paper chip, linearity between *arsM* abundance and pH, and nonlinear correlation analysis between *arsM* abundance and Se (PDF)

AUTHOR INFORMATION

Corresponding Authors

Kang Mao − *State Key Laboratory of Environmental Geochemistry, Institute of Geochemistry, Chinese Academy of Sciences, Guiyang 550081, China;* orcid.org/0000-0002-1777-5959; Email: maokang@mail.gyig.ac.cn

Hua Zhang − *State Key Laboratory of Environmental Geochemistry, Institute of Geochemistry, Chinese Academy of Sciences, Guiyang 550081, China;* orcid.org/0000-0003-4326-7875; Email: zhanghua@mail.gyig.ac.cn

Authors

Haorui Cao − *State Key Laboratory of Environmental Geochemistry, Institute of Geochemistry, Chinese Academy of Sciences, Guiyang 550081, China; University of Chinese Academy of Sciences, Beijing 100049, China*

Jiajia Yang − *State Key Laboratory of Environmental Geochemistry, Institute of Geochemistry, Chinese Academy of Sciences, Guiyang 550081, China*

Qingqing Wu − *State Key Laboratory of Environmental Geochemistry, Institute of Geochemistry, Chinese Academy of Sciences, Guiyang 550081, China; University of Chinese Academy of Sciences, Beijing 100049, China*

Jiming Hu − *College of Chemistry and Molecular Sciences, Wuhan University, Wuhan 430072, China*

Complete contact information is available at: https://pubs.acs.org/10.1021/acs.analchem.3c05958

Notes

The authors declare no competing financial interest.

ACKNOWLEDGMENTS

The authors acknowledge the Youth Cross Team Project of CAS (JCTD-2021-17), Guizhou Provincial Science and Technology Projects (Qiankehe Platform Talents-GCC [2023] 046, Qiankehe Jichu-ZK [2022] Yiban 565), National Natural Science Foundation of China (42377456 and 42107486), Guizhou Provincial 2021 Science and Technology Subsidies (no. GZ2021SIG), and Youth Innovation Promotion Association CAS (2023415).

REFERENCES

(1) Roberts, L. C.; Hug, S. J.; Dittmar, J.; Voegelin, A.; Kretzschmar, R.; Wehrli, B.; Cirpka, O. A.; Saha, G. C.; Ashraf Ali, M.; Badruzzaman, A. B. M. *Nat. Geosci.* **2010**, *3* (1), 53−59.

(2) Chatterjee, D.; Halder, D.; Majumder, S.; Biswas, A.; Nath, B.; Bhattacharya, P.; Bhowmick, S.; Mukherjee-Goswami, A.; Saha, D.; Hazra, R.; et al. *Water Res.* **2010**, *44* (19), 5803−5812.

(3) Halder, D.; Biswas, A.; Šlejkovec, Z.; Chatterjee, D.; Nriagu, J.; Jacks, G.; Bhattacharya, P. *Sci. Total Environ.* **2014**, *497−498*, 200−208.

(4) Van de Wiele, T.; Laing, G. D.; Calatayud, M. *Curr. Opin. Food Sci.* **2015**, *6*, 1−6.

(5) Podgorski, J.; Berg, M. *Science* **2020**, *368* (6493), 845.

(6) Zhu, Y. G.; Yoshinaga, M.; Zhao, F. J.; Rosen, B. P. Earth Abides Arsenic Biotransformations. In *Annual Review of Earth and Planetary Sciences, Vol 42*, Jeanloz, R., Ed.; Annual Review of Earth and Planetary Sciences, Vol. *42*; 2014; pp 443.

(7) Jia, Y.; Huang, H.; Zhong, M.; Wang, F. H.; Zhang, L. M.; Zhu, Y. G. *Environ. Sci. Technol.* **2013**, *47* (7), 3141−3148.

(8) Wang, Y.; Li, P.; Jiang, Z.; Liu, H.; Wei, D.; Wang, H.; Wang, Y. *Ecotoxicology* **2018**, *27* (8), 1047−1057.

(9) Turpeinen, R.; Pantsar-Kallio, M.; Häggblom, M.; Kairesalo, T. *Sci. Total Environ.* **1999**, *236* (1), 173−180.

(10) Qin, J.; Rosen, B. P.; Zhang, Y.; Wang, G.; Franke, S.; Rensing, C. *Proc. Natl. Acad. Sci. U. S. A.* **2006**, *103* (7), 2075−2080.

(11) Hirano, S.; Kobayashi, Y.; Cui, X.; Kanno, S.; Hayakawa, T.; Shraim, A. *Toxicol. Appl. Pharmacol.* **2004**, *198* (3), 458−467.

(12) Zhao, F. J.; Zhu, Y. G.; Meharg, A. A. *Environ. Sci. Technol.* **2013**, *47* (9), 3957−3966.

(13) Huang, J.-H.; Hu, K.-N.; Decker, B. *Water, Air, & Soil Pollution* **2011**, *219* (1), 401−415.

(14) Zhao, F. J.; Harris, E.; Yan, J.; Ma, J. C.; Wu, L. Y.; Liu, W. J.; McGrath, S. P.; Zhou, J. Z.; Zhu, Y. G. *Environ. Sci. Technol.* **2013**, *47* (13), 7147−7154.
(15) Yin, X. X.; Chen, J.; Qin, J.; Sun, G. X.; Rosen, B. P.; Zhu, Y. G. *Plant Physiol.* **2011**, *156* (3), 1631−1638.
(16) Afroz, H.; Su, S. M.; Carey, M.; Meharg, A. A.; Meharg, C. *Environ. Sci. Technol.* **2019**, *53* (7), 3451−3463.
(17) Reid, M. C.; Maillard, J.; Bagnoud, A.; Falquet, L.; Le Vo, P.; Bernier-Latmani, R. *Environ. Sci. Technol.* **2017**, *51* (18), 10546−10554.
(18) Deng, Y.; Zhou, T.; Peng, Y.; Wang, M.; Xiang, L.; Zhang, Y.; Li, J.; Yang, J.; Li, G. *Anal. Chem.* **2023**, *95* (6), 3358−3362.
(19) Faino, L.; Thomma, B. *Trends Plant Sci.* **2014**, *19* (5), 288−291.
(20) Cao, H. R.; Mao, K.; Ran, F.; Xu, P. Q.; Zhao, Y. R.; Zhang, X. Y.; Zhou, H. R.; Yang, Z. G.; Zhang, H.; Jiang, G. B. *Environ. Sci. Technol.* **2022**, *56* (18), 13245−13253.
(21) Vukomanovic, M.; Torrents, E. *J. Nanobiotechnol.* **2019**, *17* (1), 21.
(22) Li, Y.; Li, S. Y.; Wang, J.; Liu, G. *Trends Biotechnol.* **2019**, *37* (7), 730−743.
(23) Chen, J. S.; Ma, E.; Harrington, L. B.; Da Costa, M.; Tian, X.; Palefsky, J. M.; Doudna, J. A. *Science* **2018**, *360* (6387), 436−439.
(24) Broughton, J. P.; Deng, X.; Yu, G.; Fasching, C. L.; Servellita, V.; Singh, J.; Miao, X.; Streithorst, J. A.; Granados, A.; Sotomayor-Gonzalez, A.; et al. *Nat. Biotechnol.* **2020**, *38* (7), 870−874.
(25) Chen, Y.; Mei, Y. X.; Zhao, X. H.; Jiang, X. Y. *Anal. Chem.* **2020**, *92* (21), 14846−14852.
(26) Huang, D.; Zhao, Y.; Fang, M.; Shen, P.; Xu, H.; He, Y.; Chen, S.; Si, Z.; Xu, Z. *Lab Chip* **2023**, *23* (19), 4265−4275.
(27) Cao, H.; Mao, K.; Zhang, H.; Wu, Q.; Ju, H.; Feng, X. *Sci. Total Environ.* **2024**, *909*, No. 168536.
(28) Hu, M.; Qiu, Z.; Bi, Z.; Tian, T.; Jiang, Y.; Zhou, X. *Proc. Natl. Acad. Sci. U.S.A.* **2022**, *119*, 26.
(29) Huyke, D. A.; Ramachandran, A.; Bashkirov, V. I.; Kotseroglou, E. K.; Kotseroglou, T.; Santiago, J. G. *Anal. Chem.* **2022**, 9826.
(30) Li, H.; Xie, Y.; Chen, F.; Bai, H.; Xiu, L.; Zhou, X.; Guo, X.; Hu, Q.; Yin, K. *Chem. Soc. Rev.* **2023**, *52* (1), 361−382.
(31) Zeng, M. C.; Ke, Y. Q.; Zhuang, Z. Y.; Qin, C.; Li, L. Y.; Sheng, G. Y.; Li, Z. R.; Meng, H.; Ding, X. T. *Anal. Chem.* **2022**, *94* (30), 10805−10812.
(32) Luo, T.; Li, J. C.; He, Y.; Liu, H.; Deng, Z. W.; Long, X.; Wan, Q. Q.; Ding, J. C.; Gong, Z.; Yang, Y. J.; et al. *Anal. Chem.* **2022**, *94* (17), 6566−6573.
(33) English, M. A.; Soenksen, L. R.; Gayet, R. V.; de Puig, H.; Angenent-Mari, N. M.; Mao, A. S.; Nguyen, P. Q.; Collins, J. J. *Science* **2019**, *365* (6455), 780−785.
(34) Sheng, A.; Yang, J.; Tang, L.; Niu, L.; Cheng, L.; Zeng, Y.; Chen, X.; Zhang, J.; Li, G. *Nucleic Acids Res.* **2022**, *50* (18), 10562−10570.
(35) Chen, Y.; Yang, T.; Qian, S.; Peng, C.; Wang, X.; Wang, T.; Che, Y.; Ji, F.; Wu, J.; Xu, J. *Anal. Chim. Acta* **2022**, *1231*, No. 340417.
(36) Liu, P.-F.; Zhao, K.-R.; Liu, Z.-J.; Wang, L.; Ye, S.-Y.; Liang, G.-X. *Biosens. Bioelectron.* **2021**, *176*, No. 112954.
(37) Cheng, L.; Yang, F.; Tang, L.; Qian, L.; Chen, X.; Guan, F.; Zhang, J.; Li, G. *Research* **2022**, 9826484.
(38) Choi, J. R.; Hu, J.; Tang, R.; Gong, Y.; Feng, S.; Ren, H.; Wen, T.; Li, X.; Wan Abas, W. A. B.; Pingguan-Murphy, B.; et al. *Lab Chip* **2016**, *16* (3), 611−621.
(39) Cao, H.; Mao, K.; Ran, F.; Xu, P.; Zhao, Y.; Zhang, X.; Zhou, H.; Yang, Z.; Zhang, H.; Jiang, G. *Environ. Sci. Technol.* **2022**, *56* (18), 13245−13253.
(40) Mao, K.; Zhang, H.; Yang, Z. *Environ. Sci. Technol.* **2020**, *54* (7), 3733−3735.
(41) Gong, M. M.; Sinton, D. *Chem. Rev.* **2017**, *117* (12), 8447−8480.
(42) Huang, D.; Ni, D.; Fang, M.; Shi, Z.; Xu, Z. *Anal. Chem.* **2021**, *93* (50), 16965−16973.
(43) Reboud, J.; Xu, G. L.; Garrett, A.; Adriko, M.; Yang, Z. G.; Tukahebwa, E. M.; Rowell, C.; Cooper, J. M. *Proc. Natl. Acad. Sci. U.S.A.* **2019**, *116* (11), 4834−4842.
(44) Dittmar, J.; Voegelin, A.; Roberts, L. C.; Hug, S. J.; Saha, G. C.; Ali, M. A.; Badruzzaman, A. B. M.; Kretzschmar, R. *Environ. Sci. Technol.* **2007**, *41* (17), 5967−5972.
(45) Samanta, D.; Ebrahimi, S. B.; Ramani, N.; Mirkin, C. A. *J. Am. Chem. Soc.* **2022**, *144* (36), 16310−16315.
(46) Han, Y.; Lu, J.; Wang, M.; Sun, C.; Yang, J.; Li, G. *J. Electroanal. Chem.* **2022**, *920*, No. 116576.
(47) English, M. A.; Soenksen, L. R.; Gayet, R. V.; de Puig, H.; Angenent-Mari, N. M.; Mao, A. S.; Nguyen, P. Q.; Collins, J. J. *Science* **2019**, *365* (6455), 780.
(48) Yang, Z.; Xu, G.; Reboud, J.; Ali, S. A.; Kaur, G.; McGiven, J.; Boby, N.; Gupta, P. K.; Chaudhuri, P.; Cooper, J. M. *ACS Sens* **2018**, *3* (2), 403−409.

https://doi.org/10.1021/acs.analchem.3c05958
Anal. Chem. 2024, 96, 6337−6346